Combined compression and elongation experiments and non-linear modelling of liver tissue for surgical simulation

C. Chui[1] E. Kobayashi[1] X. Chen[2] T. Hisada[2] I. Sakuma[1]

[1]Biomedical Precision Engineering Laboratory, Graduate School of Frontier Sciences, The University of Tokyo, Japan
[2]Computational Biomechanics Laboratory, Graduate School of Frontier Sciences, The University of Tokyo, Japan

Abstract—*Uniaxial stress–strain data were obtained from in vitro experiments on 20 porcine livers for compressions, elongations and cycles of compression and then elongation. There were about 70 cylindrical samples, with diameter 7 mm and varying height (4–11 mm). The combined compression and elongation test provide a unified framework for both compression and elongation for applications such as computer-aided surgical simulation. It enable the zero stress state of the experimental liver sample to be precisely determined. A new equation that combined both logarithmic and polynomial strain energy forms was proposed in modelling these experimental data. The assumption of incompressibility was justified from a preliminary Poisson's ratio for elongation and compression at 0.43± 0.16 and 0.47± 0.15, respectively. This equation provided a good fit for the observed mechanical properties of liver during compression–elongation cycles and for separate compressions or elongations. The root mean square errors were 91.92± 17.43 Pa, 57.55± 13.23 Pa and 29.78± 17.67 Pa, respectively. In comparison with existing strain energy functions, this combined model was the better constitutive equation. Application of this theoretical model to small liver samples and other tissues demonstrated its suitability as the material model of choice for soft tissue.*

Keywords—*Liver tissue, Compression and tensile test, Non-linear elasticity, Mechanical properties, Computer-aided surgery*

Med. Biol. Eng. Comput., 2004, **42**, 787–798

1 Introduction

UNDERSTANDING THE biomechanics of the liver is important for developing computer simulations that could assist in the invention of new medical devices and procedures, as well as in surgical pre-treatment, planning and training (HAWKES *et al.*, 2003). The properties of materials are specified by equations. Within certain limits of stress and strain rates, many engineering structural materials can be described by idealised equations, such as those for the Hookean elastic solid. However, most biological materials, including human liver, cannot be described so simply. In this paper, we present our investigation that attempts to determine better constitutive equations for porcine liver tissues from uniaxial compression and elongation experiments.

Correspondence should be addressed to Dr Cheekong Chui; email: cheekong@miki.pe.u-tokyo.ac.jp

Paper received 27 November 2003 and in final form 28 April 2004
MBEC online number: 20043941

A constitutive equation describes a physical property of a material. Its derivation should begin with empirical measurements. There are two alternatives for constitutive modelling: the continuum approach and the microstructure approach. With the first approach, the material is assumed to be a continuum. The relevant variables are identified, and these are related in a framework that ensures invariance under a change of frames. This was our approach in this paper.

One of the earliest reported mathematical/experimental treatments of biological materials in the context of large deformation and modern continuum mechanics was that of Ticker and Sacks, in 1964 and 1967, according to VOSSOUGHI (1995). Since then, a number of constitutive models have appeared that described the passive material properties of both hard and soft tissues. However, few deal with abdominal tissues such as the liver. If the material is linear, and the deformation is limited and infinitesimal, then a simple linear relationship according to Hooke's law might be sufficient uniquely to describe the stress–strain relationship. For a non-linear material capable of undergoing large deformations, the formulation is not unique. One constitutive model may well represent one type of soft tissue but not the others, or a model may well approximate

a portion of the stress–strain curve, but not the entire space. The numerical complexity of these non-linear functions is also an issue for interactive computing using currently available computer hardware and software.

In DAVIES *et al.* (1999; 2002) and CARTER *et al.* (2001), the authors described biomechanical modelling with experimental indentations of animal abdominal organs, including liver. Their study assumed that the tissues were isotropic, homogeneous and incompressible. A non-linear constitutive model based on a strain energy polynomial function was used in MILLER (2000) to model liver and kidney. The experimental data were from *in vivo* experiments on Rhesus monkeys (MELVIN *et al.*, 1973). The experiments approximated uniaxial compression under high strain rates typical of car crashes. These non-linear models were numerically complex and not suitable for realistic, fast medical simulation. In BRUYNS and OTTENSMEYER (2002), the authors described *in vitro* testing of rat organ tissue using indentation and utilised the finite element method to derive as initial estimation of Young's modulus for the tissue. A linear elastic model was assumed in this case for fast computation.

Liver is very unique in its micro-anatomy relative to hepatic arterial, portal venous (unique dual-input supply) and hepatic venous blood with interconnecting lobular sinusoidal anatomy. Other organs behave differently when distended with blood under normal vascular pressures. It was necessary to have an in-depth investigation into the biomechanical properties of liver on its own. To date, YAMADA (1970) provides the most popular data on the mechanical properties of animal tissues.

We first describe the theory of non-linear constitutive equations and our framework. A strain energy function was used in the derivation of non-linear constitutive equations from uniaxial experiments. There are also other constitutive equations that have no apparent relationship with energy functions. These tend to be limited to the uniaxial state of stress–strain and, hence, are not reported in this paper. The energy-based equations are generally applicable in multiaxial-based formulations. The common energy functions frequently used by various investigators have polynomial, exponential, power or logarithmic forms. A good survey of the various forms of strain energy equations can be found in VOSSOUGHI (1995).

In this paper, we proposed a new constitutive equation based on a combined polynomial–logarithmic energy function. We discuss our theoretical framework and describe our uniaxial experiments. *In vitro* uniaxial experiments have long been used to characterise the biomechanical properties of living tissues. Tissue samples were extracted and usually subjected to either compression tests or elongation tests. However, we performed combined compression and elongation testing in addition to these conventional tests. In addition to providing the most relevant, unified framework for both compression and elongation for applications such as computer-integrated surgical simulation, this test enables the zero-stress state to be precisely determined.

Based on our experimental data, a comprehensive set of strain energy functions were investigated to determine their suitability for representing the biomechanical properties of liver. Our observations and new model were further validated with separate experiments using smaller liver samples. The new combined logarithmic and polynomial model was also used to model a compression and then elongation experiment on porcine kidney and brain tissues.

2 Theories of non-linear constitutive relationships

A well-known approach for studying non-linear constitutive relationships of bodies capable of finite deformation is to postulate that elasticity has the form of an elastic potential, or strain energy function, W. The strain energy for an elastic body is a function of the state of deformation.

Let $\boldsymbol{X}$ denote a point in the reference configuration. The current position of the point is denoted by $\boldsymbol{x}$, where $\boldsymbol{x}$ is a function of time. The gradient of $\boldsymbol{x}$ with respect to $\boldsymbol{X}$ is called the deformation gradient

$$\boldsymbol{F} = \left(\frac{\partial \boldsymbol{x}}{\partial \boldsymbol{X}}\right)^T \tag{1}$$

The right Cauchy–Green tensor $\boldsymbol{C}$ is a measure of the strain the body experiences

$$\boldsymbol{C} = \boldsymbol{F}^T\boldsymbol{F} \tag{2}$$

The constitutive assumption of non-linear elasticity is that the stress tensor at point $\boldsymbol{x}$ depends only on the material and the deformation gradient at $\boldsymbol{x}$. If the mechanical properties do not depend explicitly on the particular point $\boldsymbol{x}$, the material is said to be homogeneous. We have assumed that liver tissue is homogeneous in our investigation.

When a quantity is unchanged with a frame rotation, it is said to be invariant. From $\boldsymbol{C}$, which is a second-order tensor, three scalar invariants can be formed by taking the trace of $\boldsymbol{C}$, $\boldsymbol{C}^2$ and $\boldsymbol{C}^3$. They are

$$I = \text{trace}(\boldsymbol{C}) = C_{ii},\ II = \text{trace}(\boldsymbol{C}^2) = C_{ij}C_{ji} \text{ and}$$
$$III = \text{trace}(\boldsymbol{C}^3) = C_{ij}C_{jk}C_{ki}$$

However, it is customary to use strain invariants defined as follows:

$$I_1 = I,\ I_2 = \frac{1}{2}(I^2 - II) \text{ and } I_3 = \frac{1}{6}(I^3 - 3I \cdot II + 2III)$$
$$= \det(\boldsymbol{C})$$

Assuming that liver is isotropic, the strain energy function can be expressed as a function of the above strain invariants, $W(I_1, I_2, I_3)$. We denote λ_i as the principal values of $\boldsymbol{F}$, and I_i is a function of λ_i.

$$\boldsymbol{F} = \begin{pmatrix} \lambda_1 & & \\ & \lambda_2 & \\ & & \lambda_3 \end{pmatrix} \tag{3}$$

As liver is known to comprise highly incompressible material, $\det\boldsymbol{F} = \lambda_1\lambda_2\lambda_3 = 1$. Under uniaxial deformation, the cross-sectional area of the cylindrical sample reduces by $1/\lambda$ when the height of the sample is increased by a factor of λ. By setting $\lambda = \lambda_3$, we have $\lambda_1 = \lambda_2 = 1/\sqrt{\lambda_3}$. Invariants I_1, I_2 and I_3 under uniaxial deformation can be evaluated as $I_1 = \lambda^2 + 2/\lambda$, $I_2 = 2\lambda + 1/\lambda^2$ and $I_3 = 1$, respectively.

For an elastic material, the second Piola–Kirchhoff stress tensor $\boldsymbol{S}$ can be expressed in terms of strain energy W and Green–Lagrange strain tensor $\boldsymbol{E}$ as follows:

$$\boldsymbol{S} = \frac{\partial W}{\partial \boldsymbol{E}} = 2\frac{\partial W}{\partial \boldsymbol{C}} \tag{4}$$

The Cauchy stress σ is related to $\boldsymbol{S}$ by

$$\sigma = \frac{1}{J}\boldsymbol{F} \cdot \boldsymbol{S} \cdot \boldsymbol{F}^T \tag{5}$$

where $J = \det\boldsymbol{F}$.

We can now express a component of σ in the tensile or compressive direction as a partial derivative of W by the invariants

$$\sigma = 2\frac{\partial W}{\partial I_1}\left(\lambda^2 - \frac{1}{\lambda}\right) + 2\frac{\partial W}{\partial I_2}\left(\lambda - \frac{1}{\lambda^2}\right) \tag{6}$$

As Cauchy stress σ is related to the first Piola–Kirchhoff stress tensor $\boldsymbol{T}$ by

$$\sigma = \frac{1}{J}\boldsymbol{F} \cdot \boldsymbol{T} \tag{7}$$

we can deduce that $\sigma = \lambda T$.

From (6),

$$T = \frac{2}{\lambda}\frac{\partial W}{\partial I_1}\left(\lambda^2 - \frac{1}{\lambda}\right) + \frac{2}{\lambda}\frac{\partial W}{\partial I_2}\left(\lambda - \frac{1}{\lambda^2}\right) \tag{8}$$

Suppose that the original cross-sectional area of the cylindrical sample used in our experiment is A_0 and the tensile or compressive load is F, then

$$T = \frac{F}{A_0} \tag{9}$$

If the original length of the cylindrical sample is L_0, the displacement

$$\Delta L = L_0(\lambda - 1) \tag{10}$$

T in (9) is measured using a precise instrument described in the following section. The instrument also concurrently measures the displacement in (10). By comparing the experimental curve obtained by plotting T against λ with the theoretical curve from (8), obtained using various strain energy functions, we seek to determine the strain energy function that can best represent the material behaviour of porcine liver tissue.

Strain energy functions have long been proposed for modelling the mechanical behaviour of biological materials and tissues. For solid biomechanics, most of the work has concentrated on blood vessels and myocardium. There are fewer reports of work on lung, skin, ligament, tendon, cartilage and bone tissue. To the best of our knowledge, there is as yet no strain energy-based constitutive relationship that is derived from extensive measurements on liver. Our assumption for the isotropic, homogeneous and incompressible liver model is consistent with recent literature (SCHMIDLIN *et al.*, 1996; FARSHAD *et al.*, 1998; MILLER, 2000; CARTER *et al.*, 2001; DAVIES *et al.*, 2002) on modelling of abdominal organs for surgical simulation.

2.1 *Polynomial strain energy functions*

The Mooney–Rivlin material is an example of a strain energy function with polynomial form (MOONEY, 1940). The Mooney–Rivlin material has been adequate for most qualitative engineering purposes in modelling hyperelastic solids such as rubber.

Using the following Mooney–Rivlin energy function with nine material constants (known as the nine-constant theory),

$$\begin{aligned} W = {} & C_1(I_1 - 3) + C_2(I_2 - 3) + C_3(I_1 - 3)^2 \\ & + C_4(I_1 - 3)(I_2 - 3) + C_5(I_2 - 3)^2 + C_6(I_1 - 3)^3 \\ & + C_7(I_1 - 3)^2(I_2 - 3) + C_8(I_1 - 3)(I_2 - 3)^2 \\ & + C_9(I_2 - 3)^3 \end{aligned} \tag{11}$$

where C_1, C_2, C_3, C_4, C_5, C_6, C_7, C_8 and C_9 are material constants.

We derived the stress–strain relationship from (8). The resulting equation was highly complex, with the highest-order term having a power of 6 and the lowest-order term having a power of -5.

Equation (12) is the two-constant version of the energy function for the Mooney–Rivlin material

$$W = \frac{C_1}{2}(I_1 - 3) + \frac{C_2}{2}(I_2 - 3) \tag{12}$$

where C_1 and C_2 are material constants, and $C_1, C_2 > 0$.

Partial differentiation of W in (12), with I_1 and I_2 obtained from (8), yielded the following stress–strain relationship. Note that λ is equal to strain plus 1. For ease of discussion, we simply refer to $T = f(\lambda)$ as the stress–strain relationship.

$$T = C_1\lambda + C_2 - \frac{C_1}{\lambda^2} - \frac{C_2}{\lambda^3} \tag{13}$$

Using non-linear curve fitting, we could evaluate how well this stress–strain relationship represented the experimental data.

The simplest polynomial-based energy function is the neo-Hookean model, which was originally applied to incompressible non-linear elastic engineering materials. The neo-Hookean model is a subset of the Mooney–Rivlin model with $C_2 = 0$. There is only one material constant C_1 in this equation (14).

$$W = C_1(I_1 - 3) \tag{14}$$

2.2 *Exponential and logarithmic strain energy functions*

Equation (15) is an exponential form of strain energy due to FUNG (1967) and DEMIRAY (1972)

$$W = \frac{C_1}{2C_2}(e^{C_2(I_1 - 3)} - 1) \tag{15}$$

where C_1 and C_2 are material constants, and $C_1, C_2 > 0$.

Partially differentiating W in (15) with I_1 and $\partial W/\partial I_2 = 0$, we obtained from (8) the stress–strain relationship.

In VERONDA and WESTMANN (1970), the authors proposed the following energy function:

$$W = C_1(e^{C_3(I_1 - 3)} - 1) + C_2(I_2 - 3) + g(I_3)$$

As we assumed that liver tissue is incompressible, $g(I_3) = 0$.

$$W = C_1(e^{C_3(I_1 - 3)} - 1) + C_2(I_2 - 3) \tag{16}$$

For cat's skin, VERONDA and WESTMANN (1970) suggested the following values for the material constants: $C_1 = 0.00394$, $C_2 = -0.01985$, $C_3 = 5.03$. Partially differentiating W in (8) with I_1 and I_2, we obtained from (16) the stress–strain relationship.

A related class of exponential equations with logarithmic form was proposed by Hayashi and Takamizawa (TAKAMIZAWA and HAYASHI, 1987; HAYASHI, 1993). They concluded from their investigations that the logarithmic form is far superior to the polynomial form and somewhat better than the exponential form. The equation was intended for transversely anisotropic material. We proposed the following logarithmic equation for isotropic material:

$$W = -C_1 \ln(1 - C_2(I_1 - 3)) \tag{17}$$

The main difference between (17) and the original Hayashi equation is the absence of invariant I_4 in the former. This invariant was not applicable with an isotropic material. We assumed that liver is an isotropic material in this paper. The original equation of Hayashi was listed as

$$\begin{aligned} W = -C_1 \ln\Big(1 & - \frac{1}{2}C_2(I_1 - 3)^2 + \frac{1}{2}C_3(I_4 - 1)^2 \\ & + C_4(I_1 - 3)(I_4 - 1)\Big) \end{aligned}$$

2.3 *Equations from power law stress–strain model*

The fourth type of commonly used constitutive relationship is the power law of the form $T = KS^n$, where T is the Lagrangian stress tensor, S is the strain or strain rate tensor, and K and n are the material constants. The advantage of the power law stress–strain function is its simplicity. Equation (18) was

originally proposed by TANAKA and FUNG (1974). It was used to model the zero-stress state of blood vessel walls in XIE *et al.* (1995).

$$T = C_1(\lambda - 1)^{C_2} \tag{18}$$

The power law energy function has also been used extensively in mechanical engineering. The Odgen model, as described in HISADA and NOGUCHI (1995), for example, was originally proposed for incompressible, rubber-like materials. In ZOBITZ *et al.* (2001), the extrafibrillar matrix of tendon material was formulated as a hyperelastic material using the Odgen form of strain energy function.

$$W = \sum_{n=1}^{3} \frac{C_n}{\alpha_n}(\lambda_1^{0.5\alpha_n} + \lambda_2^{0.5\alpha_n} + \lambda_3^{0.5\alpha_n})$$

$$T = \sum_{n=1}^{3} \frac{C_n}{2}(\lambda^{\alpha_n} - \lambda^{0.5\alpha_n - 1}) \tag{19}$$

A variant of the Odgen model was proposed in BOGEN (1987) to describe passive myocardial behaviour where C_1 and C_2 are material constants. The equations were as follows:

$$W = \frac{C_1}{C_2}(\lambda_1^{C_2} + \lambda_2^{C_2} + \lambda_3^{C_2} - 1)$$

$$\sigma = C_1(\lambda^{C_2} + \lambda^{-2C_2}) \tag{20}$$

The Cauchy stress σ is related to first Piola–Kirchhoff stress T by (7). Hence, the first Piola–Kirchhoff form of the Bogen equation used in our studies is

$$T = C_1(\lambda^{C_2 - 1} + \lambda^{-2C_2 - 1}) \tag{21}$$

2.4 *Combined energy functions*

We observed in our preliminary investigations that stress–strain equations derived from the polynomial strain energy function could fit the complete compression and elongation cycle. However, these equations generally have higher standard errors compared with exponential functions when used to represent independent compression or elongation. It is therefore meaningful to combine the exponential and polynomial strain energy functions to produce a more representative constitutive equation.

The first reported attempt to apply the combined equation was in FUNG *et al.* (1993). FUNG *et al.* proposed a strain energy expression that combined polynomial and exponential forms. This expression followed from their finding that linear (Hooke's law), exponential and power law models did not fit the entire stress–strain curve obtained from their experiments with canine thoracic aorta. As HAYASHI (1993) reported that the logarithmic form of strain energy function was somewhat better than the exponential form, and our preliminary investigation also revealed that the logarithmic form was indeed better, we focussed on the combined logarithmic and polynomial model here. The application of the combined exponential and polynomial equations is not reported in this paper.

The combined logarithmic and polynomial model can be derived in the same spirit as the derivation in FUNG *et al.* (1993). At low strain, the logarithmic component in the combined model was small, and the polynomial component was the dominant one. Their roles were reversed at high strain. The combined logarithmic and polynomial model is therefore advantageous in describing the entire stress–strain curve. Note that the Veronda and Westmann model (16) also has both exponential and polynomial terms. The Veronda and Westmann model was a sum of an exponential function and a polynomial originally for constitutive modelling of the skin. It did not have the numerical advantages described above from combining the strengths of exponential and polynomial forms. Equation (22) is our proposed combined logarithmic and polynomial equation for isotropic materials

$$W = \frac{-C_1}{2}\ln(1 - C_2(I_1 - 3)) + C_3(I_1 - 3) \tag{22}$$

To simplify the discussion, we have referred to this equation as the combined logarithmic and polynomial model.

3 Materials and methods

The recent interest and progress in measuring the mechanical properties of tissues have been fuelled by developments in computer-integrated surgery, where precise information about the elastic properties of living tissues is desired. Surgical instruments have been equipped with force-sensing capabilities, allowing elasticity measurement during surgery (CARTER *et al.*, 2001; MUTHUPILLAI *et al.*, 1995). PATHAK *et al.* (1998) applied indentation methods for *in vivo* experiments on the skin. However, these techniques lacked well-defined boundary conditions during the experiment and often failed to address the complex material properties of tissue with nonlinear constitutive equations.

MR elastography (KYRIACOU *et al.*, 1996) was a possible method for non-invasive imaging of elastic properties in non-homogeneous organs. This method spatially maps and quantifies small displacements caused by propagating harmonic mechanical waves. Nevertheless, the resulting very small displacements and frequency range could not predict the tissue behaviour in the range of strains and strain rates observed during surgical interventions.

Uniaxial tests have long been used to measure the mechanical properties of both soft and hard tissues (YAMADA, 1970). MILLER and CHINZEI (1997) described a uniaxial compression test to measure the mechanical properties of brain tissue. We reported our preliminary work on uniaxial experiments with porcine liver in SAKUMA *et al.* (2003). Indentation tests were used in DAVIES *et al.* (2002) to determine the mechanical properties of spleen tissue. To simulate the deformation of liver tissue more realistically, we needed precise measurements of the mechanical behaviour from compression and elongation experiments. Hence, in addition to performing the conventional compression and elongation tests on liver tissue, we measured the force-displacement during a cycle of compression and elongation. This combined compression and elongation test also enabled the zero-stress state to be precisely determined for the tension test.

We found that, by compressing a cylindrical liver sample of diameter 7 mm with a force of less than 1 N, we could start the tension test at the zero-stress and -strain state. In our other work on investigating the strength of liver, we found that the yield stress and strain were approximately 2.5×10^5 Pa and 69.5% for compression. With this yield stress, the compressive stress achieved by 1 N was one order of magnitude less than the yield stress. We also found that the resultant force-displacement relationship before and after preconditioning did not change with 1 N of preconditioning load. The combined compression and elongation cycle was clearly a simpler method compared with the use of lasers for initial state estimation (MILLER and CHINZEI, 1997).

Fresh porcine livers were purchased from a local slaughterhouse for these experiments. It is generally believed that the mechanical properties of pig liver are close to those of human liver. The weight of a whole porcine liver was 1.5 ± 0.2 kg. Test samples were cylindrical in shape, with a fixed diameter of 7 mm and heights ranging from 4.5 mm to 11 mm.

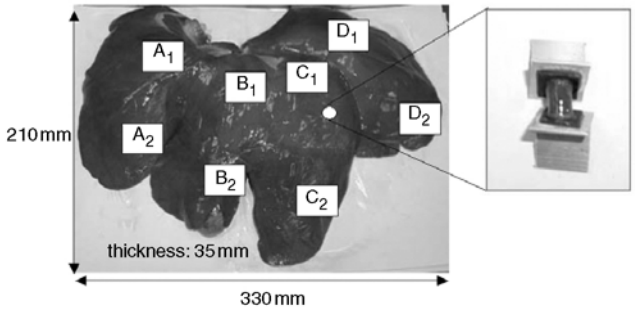

Fig. 1 *Whole porcine liver with test sample. Eight groups of samples were extracted from different locations (A_1, A_2, B_1, B_2, C_1, C_2, D_1, D_2) in liver. Average mass densities at these locations were 1.070, 1.078, 1.030, 1.074, 1.058, 1.074, 1.074 and 1.057 g cm^{-3}, respectively*

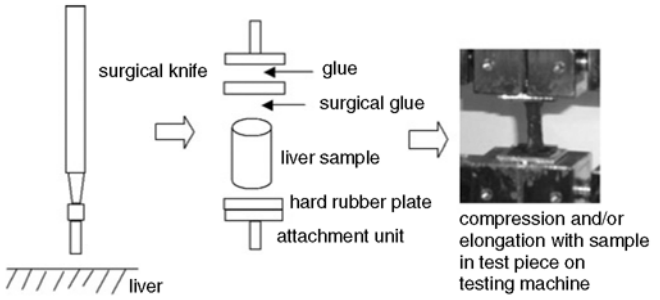

Fig. 2 *Overview of experimental procedure. Sequence flows from left to right. Sample was first extracted from liver surface. Test unit was made and placed under testing machine for experiments*

Fig. 1 shows a typical whole liver and one of the liver samples used in the experiments. Before testing, samples were visually inspected for visible vessels and large pores. We looked for vessels from all sides of the sample. Those samples with vessels or obvious pores were discarded. As the samples were rather small, at 7 mm diameter, and generally less than 10 mm in height, and because they were extracted near the liver surface, we were quite certain that the presence of a vessel in the sample was not significant, even if missed by the inspection.

The density of porcine liver referred to or implied mass density and was determined by dividing the measured weight of the specimen by its volume. The volume of the cylindrical sample was easily determined, as its radius and height were measured during the preparation. Digital scales were used to weigh the sample before and after the experiments. We assumed that liver tissue was isotropic. A digital video camera was placed in front of the sample and recorded the deformation during the experiment. From the recorded planar images, we calculated the area of the sample, based on the number of pixels. The area remained roughly constant before, during and after the various experiments. The difference in area at any recorded instant of the experiment was at most 2%. As there was no change in weight before and after the experiment, we assumed that the density, and specifically the weight of the liver, did not change before, after and during the various experiments. Additionally, based on a study of 24 elongation and 15 compression experiments, we determined that the Poisson's ratios for elongation and compression were 0.43 ± 0.16 and 0.47 ± 0.15, respectively. Hence, the porcine liver tissue sample was possibly incompressible. This is an important condition for the application of the various energy based constitutive models described in Section 2.

Fig. 2 illustrates the experimental procedure. The tissue sample to be tested was extracted from the pig liver using a disposable surgical knife. Surgical bond* was used to glue the sample to the attachments. To establish maximum bonding between the tissue and the attachment unit, we tested the adhesion between liver tissue and various surfaces, including wood, steel, cloth and rubber. Adhesion to the rubber plate was maintained with the highest tension used in our experiments. This was twice that obtained using wood, which had the lowest value. At a temperature of 20 ± 3°C, the surgical bond was able to sustain a stress of up to 380 kg cm^{-2}.

Force and displacement were measured during the loading test by an Eztest precision instrument†. This instrument had a resolution of $\pm$ 1% and could support loading rates ranged from 0.5 to 1000 mm min^{-1}. We used a load cell that was capable of measuring a force up to 20 N. Experiments were performed between August and December 2002, with 70 samples taken from 20 pig livers. Environmental temperature was about 22°C. Humidity was kept between 60% and 70% to prevent drying of the test pieces. In the combined compression and elongation test, the sample was first compressed, returned to its stress-free position and then elongated. Preconditioning with periodical loading and unloading was carried out in all tests.

Note that, from the theoretical treatment above, we refer to stress and strain in the Lagrangian sense. Thus, for a one-dimensional sample loaded in tension, the tensile stress T is the load divided by the cross-sectional area of the sample at zero-stress state. The 'stretch ratio' or 'compression ratio' λ is the ratio of the length or height of the sample stretched or compressed under the load divided by the initial length at the zero-stress state.

For the investigation into the heterogeneity of porcine liver, test sample lengths of 10 ± 1 mm and loading rates of 10 mm min^{-1} were used. Fig. 3 compares the stress–strain curves from the visceral side, diaphragmatic side and edge of the liver. We observed that samples extracted from the upper surface (diaphragmatic side) of the liver were noticeably harder than those from other parts of the liver. This was possibly owing to the presence of a thin capsular layer on the liver surface. As we were mainly interested in computer-aided surgical simulation, with surgical devices such as needles approaching the liver from the top, samples extracted from the

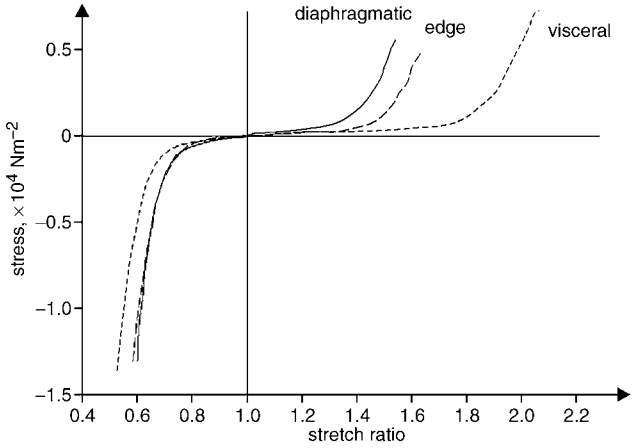

Fig. 3 *Stress–strain relationships for tissue extracted from different parts of liver. Total of 21 samples were extracted from 2 porcine livers. Diameter and height of cylindrical samples were 6–7 mm and 4–5 mm, respectively. Loading rate was 10 mm min^{-1}*

*Adhesive A, Sankyo Co. Ltd, Tokyo, Japan

†Shimadzu Co. Ltd, Japan

diaphragmatic side of the liver were used in our biomechanical analyses of liver properties.

We briefly studied the effect of temperature on the mechanical properties of liver. We compared the force-displacement curves obtained at various temperatures (22°C, 37°C and 80°C). At 80°C, the liver tissue was close to vaporisation. The material behaviour of liver tissue was essentially the same at 22°C and 37°C. As we wanted to perform as many tests as possible, experiments were conducted at room temperature (22°C).

Fig. 4 shows the stress–strain relationship of liver tissue obtained at the constant loading rates of 1, 2, 5, 10, 20, 50, 100 and 200 mm min^{-1}. These corresponded to strain rates of 0.003, 0.006 0.030, 0.061, 0.151, 0.303 and 0.606 s^{-1}, respectively. The effect of strain rate on porcine liver was shown to be relatively insignificant. Hence, in this investigation, we did not need to consider further the visco-elastic properties of porcine liver.

As has been reported for other animal tissues (FUNG, 1993), porcine liver exhibited tissue relaxation. We observed during these experiments that, when the liver sample was compressed, and then the compression was maintained, the amount of force measured by Eztest gradually decreased. At low loading rates (1–2 mm min^{-1}), some tissue relaxation was observed, whereas very fast rates (50–200 mm min^{-1}) resulted in large increments between data points. We found that the loading rate of 10 mm min^{-1} was the most suitable. This corresponded to a strain rate of between 0.041 s^{-1} and 0.015 s^{-1}, as our samples ranged in height from 4 mm to 11 mm. This was consistent with values required for our targeted application, computer-aided surgical simulation, with a low strain rate of 0.01 s^{-1} reported as typical for neurosurgery. Slightly higher strain rates were included in our study, because we needed to predict the initial response of liver to a surgical probe. In general, higher strain rates occur during abdominal surgery. By testing all samples at the same rate, the confounding effects of the relatively insignificant tissue visco-elasticity were further minimised.

4 Results and discussions

Figs 5–7 show the mean and median stress T against the stretch ratio λ curves corresponding to compression only, elongation only and combined compression and then elongation measurements, respectively. The standard deviation from the mean stress is also indicated in the respective Figure. A constitutive equation in the $T=f(\lambda)$ form is considered to fit the experimental data if the theoretical curve follows the shape of the average curve, and the standard error is small. We defined standard error as root mean square errors (RMSEs), calculated from the difference between the theoretical estimate and the experimental measurement. An error of more than 120 was considered a bad fit. The mismatch between experimental and theoretical curves was apparent with this error. We were seeking to model the entire stress–strain curve in the physiological region, up to values of about 30% strain. Models with few material parameters were preferred for the purpose of computational efficiency. Software for non-linear least-square data fitting using the Gauss–Newton method assisted us in estimating the coefficients for the non-linear functions.

Almost all the constitutive models provided good fits for the experimental data over the elongation region. The fits for the simpler models, the neo-Hookean and the Mooney–Rivlin (two-constants), were not acceptable for fitting the entire curves. The Mooney–Rivlin model with nine constants produced smaller residual errors than its simpler version. This was mainly owing to the higher-order constants. Nevertheless, there were sign changes in the values of material constants in these polynomial-based models.

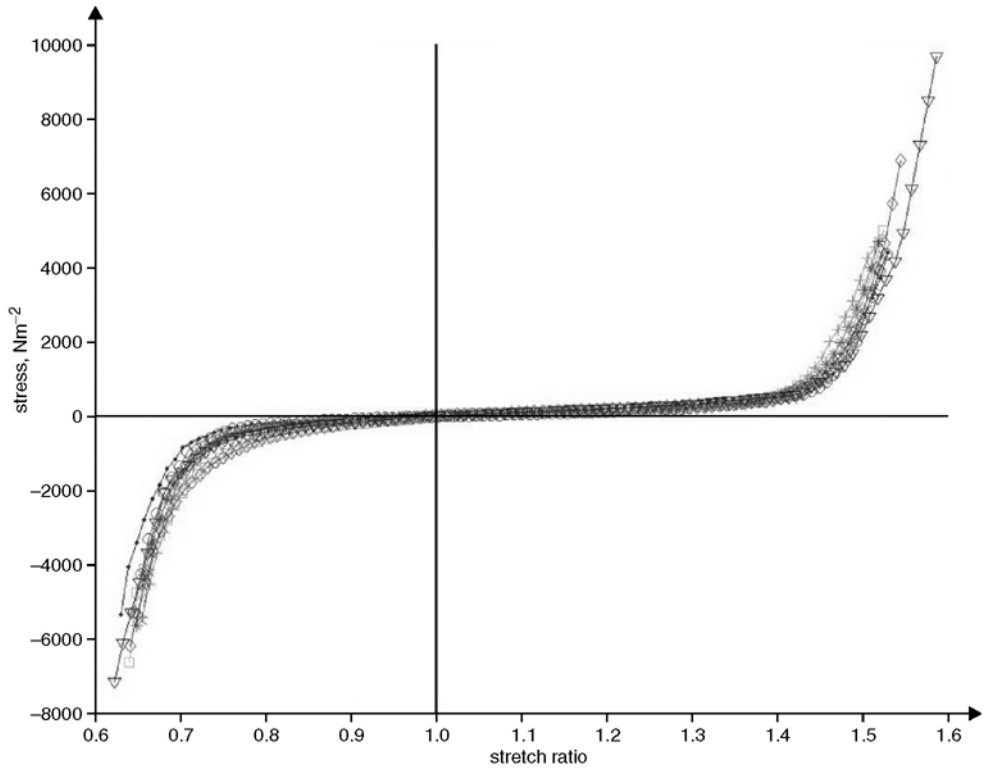

Fig. 4 *Stress–strain relationships for liver tissue obtained at various loading rates. Total of 12 samples were extracted from 1 porcine liver. Diameter and height of cylindrical samples were 7 mm and 5.5 mm, respectively. Loading rates: (–▲–) 1 mm min^{-1}; (–○–) 2 mm min^{-1}; (–+–) 5 mm min^{-1}; (–|–) 10 mm min^{-1}; (–*–) 20 mm min^{-1}; (–□–) 50 mm min^{-1}; (–◇–) 100 mm min^{-1}; (–▽–) 200 mm min^{-1}*

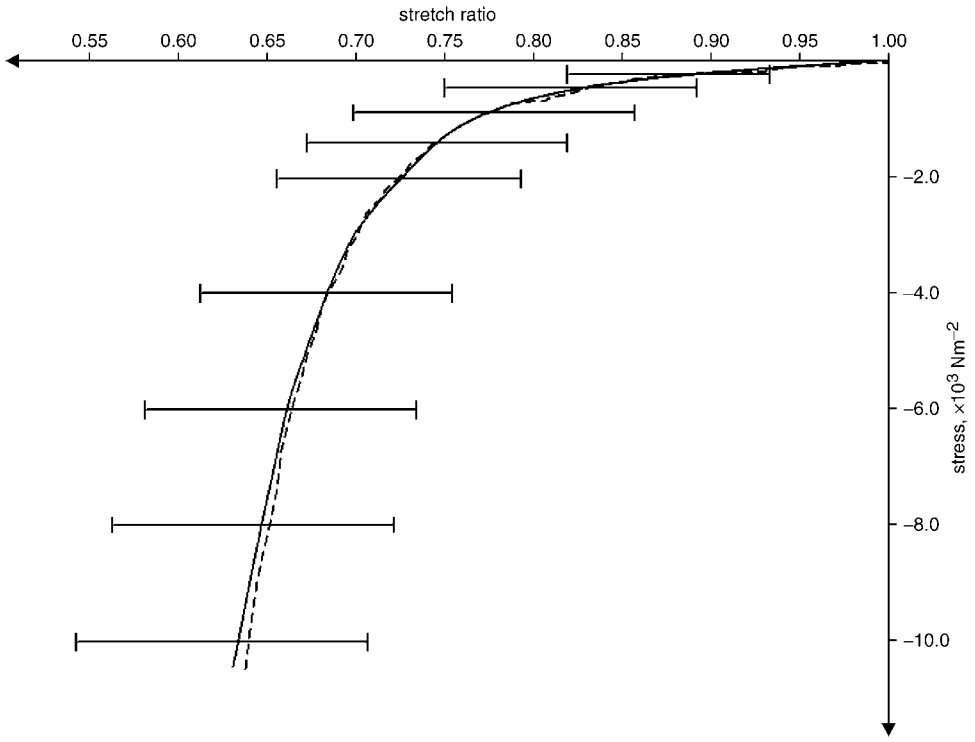

Fig. 5. *Stress (T)–stretch (λ) graphs from uniaxial compression measurements with porcine liver tissue. There were 70 samples from 20 livers. Diameter and height of cylindrical samples were 7 mm and 4–7 mm, respectively. Loading rate was 10 mm min^{-1}. (—) Mean and (—) median values of experiments. Standard deviations from mean values are indicated with horizontal bars*

Both exponential and logarithmic models were comparable in representing the experimental data, with the logarithmic models somewhat better. This is in agreement with previous reports (HAYASHI, 1993). The combined models were better than these models, with respect to their RMSEs. The average error for fitting the maximum, mean and minimum experimental data in the combined logarithmic and polynomial model was 29.78 ± 17.67 Pa. This was the next best after the Mooney–Rivlin (nine-constant) model with 26.63 ± 9.63 Pa.

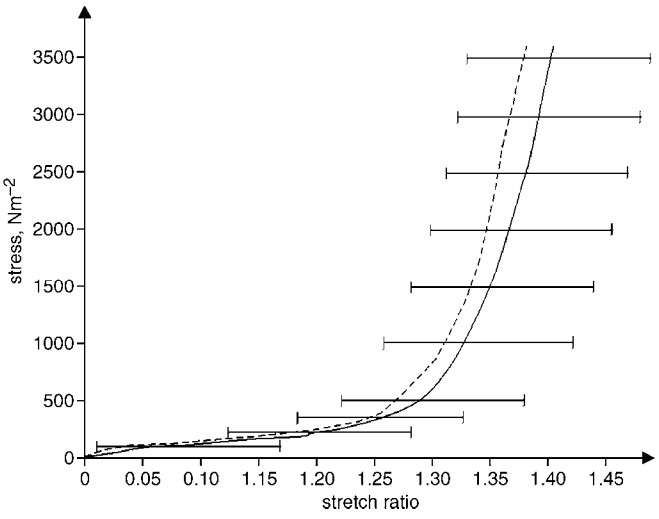

Fig. 6 *Stress (T)–stretch (λ) graphs from uniaxial elongation measurements with porcine liver tissue. There were 11 samples from 4 livers. Diameter and height of cylindrical samples were 7 mm and 8.5–11 mm, respectively. Loading rate was 10 mm min^{-1}. (—) Mean and (– –) median values of experiments. Standard deviations from mean values are indicated with horizontal bars*

The isotropic logarithmic model was third with 46.87 ± 13.74 Pa. The average error of the Veronda and Westmann model and the Fung–Demiray model were 42.91 ± 5.41 Pa and 61.86 ± 9.17 Pa, respectively. The best-fit Mooney–Rivlin (nine-constant) model had the following material constants for minimum, mean and maximum curves, respectively: $[-2.97 \times 10^4, 3.14 \times 10^4, -5.36 \times 10^4, 1.32 \times 10^4, 7.86 \times 10^4, 3.23 \times 10^4, 2.34 \times 10^4, -1.10 \times 10^4, -4.45 \times 10^4]$, $[-0.24 \times 10^4, 0.26 \times 10^4, -4.38 \times 10^4, 0.22 \times 10^4, 5.20 \times 10^4, -1.86 \times 10^4, 3.42 \times 10^4, 2.93 \times 10^4, 0.11 \times 10^4]$ and $[0.12 \times 10^4, -0.11 \times 10^4, 5.47 \times 10^4, 0.08 \times 10^4, -6.63 \times 10^4, 3.61 \times 10^4, -2.70 \times 10^4, -3.04 \times 10^4, -3.47 \times 10^4]$. The curve fit by the combined logarithmic and polynomial model was achieved using the following material constants for minimum, mean and maximum curve, respectively: [−348.51, 3.03, −328.95], [−337.77, 2.22, −287.78] and [−322.35, 1.51, −210.33].

Not all equations provided good fits for the experimental compression data. The Tanaka model could not match the compression stress–strain curve. In fact, the errors associated with power models were large. Mathematically, a power equation such as the Tanaka model could not represent compression, as the theoretical stress computed using this equation was always positive for all positive stretch ratios. The exponential and logarithmic models were comparable in representing the experimental data. The combined model was good. The Mooney–Rivlin (nine-constant) model had the smallest RMSE. The higher-degree terms of the polynomial function were responsible for the small RMSEs. The average errors for the Mooney–Rivlin (nine-constant) model and combined logarithmic and polynomial model were 48.98 ± 28.69 Pa and 57.55 ± 13.23 Pa, respectively. The average errors of the isotropic logarithmic model, Fung–Demiray model and Veronda and Westmann model were 110.2 ± 58.93, 154.3 ± 115 Pa and 154.9 ± 115 Pa, respectively. The best-fit Mooney–Rivlin (nine-constant) model had the following material constants for minimum, mean and maximum curves,

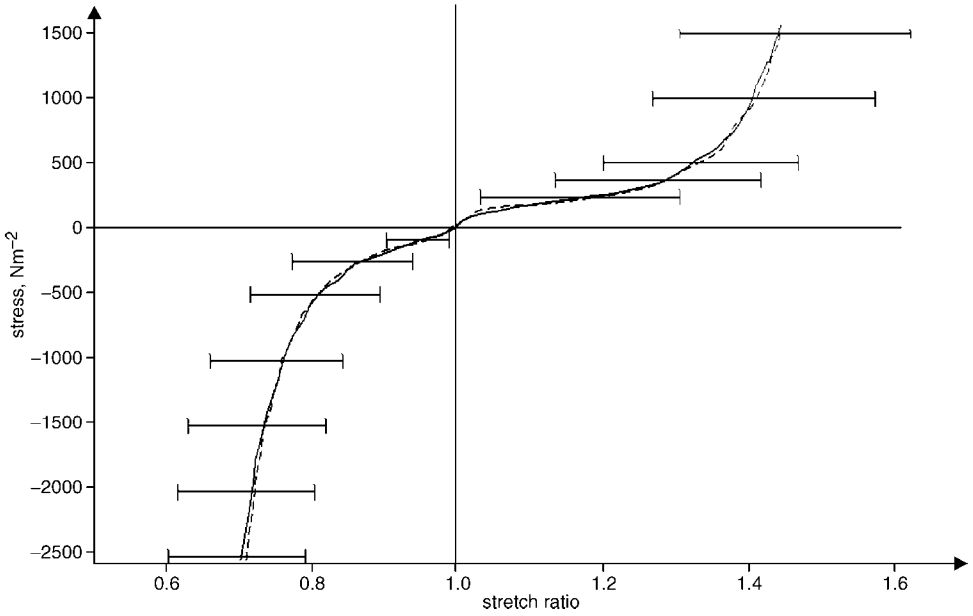

Fig. 7 *Stress (T)–stretch (λ) graphs from uniaxial combined compression and elongation measurements with porcine liver tissue. There were 65 samples from 18 livers. Diameter and height of cylindrical samples were 7 mm and 4–7 mm, respectively. Loading rate was 10 mm min^{-1}. (—) Mean and (– – –) median values of experiments. Standard deviations from mean values are indicated with horizontal bars*

respectively: $[-1.98\times10^4,\ 1.91\times10^4,\ 5.75\times10^4,\ -0.61\times10^4,\ 7.3.95\times10^4,\ 1.18\times10^4,\ 2.72\times10^4,\ 1.42\times10^4,\ -0.33\times10^4]$, $[0.03\times10^4,\ 0.0024\times10^4,\ -0.73\times10^4,\ -0.07\times10^4,\ 0.72\times10^4,\ -1.98\times10^4,\ 0.43\times10^4,\ 0.80\times10^4,\ -0.24\times10^4]$ and $[-0.27\times10^5,\ 0.26\times10^5,\ 0.96\times10^5,\ -0.09\times10^5,\ -0.91\times10^5,\ 0.28\times10^5,\ 1.09\times10^5,\ 1.45\times10^5,\ -1.21\times10^5]$. The curve fit by the combined logarithmic and polynomial model was achieved using the following material constants for minimum, mean and maximum curve, respectively: [−6767.58, 1.12, −2812.78], [−7881.10, 1.65, −3941.40] and [−9922.58, 2.42, −5936.80].

Table 1 shows the results of fitting the above constitutive equations to experimental data for compression and then elongation. Failure to match the experimental data (RMSE > 120 Pa) was partly due to the difficulties in representing both negative and positive domains numerically in

Table 1 Parameters of various models representing combined compression and then elongation experimental data. Models were ranked in accordance with average RMSE ± SD

Model	Minimum curve	Mean curve	Maximum curve	Average RMSE ± SD, Pa
Mooney–Rivlin (nine-Constants) (11)	$C_1=0.20\times10^4$	$C_1=0.16\times10^3$	$C_1=-0.23\times10^4$	38.71 ± 21.99
	$C_2=-0.15\times10^4$	$C_2=0.14\times10^3$	$C_2=0.27\times10^4$	
	$C_3=-0.61\times10^4$	$C_3=-0.12\times10^4$	$C_3=-0.99\times10^3$	
	$C_4=0.30\times10^4$	$C_4=0.62\times10^3$	$C_4=0.32\times10^4$	
	$C_5=0.19\times10^4$	$C_5=0.41\times10^3$	$C_5=-0.15\times10^4$	
	$C_6=3.16\times10^4$	$C_6=0.72\times10^4$	$C_6=1.03\times10^4$	
	$C_7=-3.35\times10^4$	$C_7=-1.43\times10^4$	$C_7=-2.18\times10^4$	
	$C_8=-0.76\times10^3$	$C_8=0.91\times10^4$	$C_8=0.31\times10^3$	
	$C_9=0.55\times10^4$	$C_9=-0.92\times10^3$	$C_9=1.40\times10^4$	
Combined logarithmic and polynomial (22)	$C_1=-457.21$	$C_1=-342.44$	$C_1=-214.73$	91.92 ± 17.43
	$C_2=9.77$	$C_2=1.99$	$C_2=4.71$	
	$C_3=-119.78$	$C_3=-136.08$	$C_3=-221.21$	
TAKAMIZAWA and HAYASHI (1987) (17)	$C_1=752.57$	$C_1=168.01$	$C_1=175.08$	134.6 ± 23.06
	$C_2=0.61$	$C_2=4.11$	$C_2=9.27$	
	$C_3=0.20$	$C_3=0.82$	$C_3=1.27$	
	$C_4=0.29$	$C_4=1.17$	$C_4=1.89$	
BOGEN (1987) (18)	$C_1=-47.87$	$C_1=-43.98$	$C_1=-83.553$	153.5 ± 50.13
	$C_2=3.90$	$C_2=5.44$	$C_2=6.4399$	
Fung–Demiray (15)	$C_1=525.32$	$C_1=670.65$	$C_1=1209.2$	187.6 ± 87.02
	$C_2=2.618$	$C_2=4.570$	$C_2=6.829$	
Veronda and Westman (16)	$C_1=99.45$	$C_1=72.62$	$C_1=87.56$	188.2 ± 87.26
	$C_2=2.62$	$C_2=4.58$	$C_2=6.84$	
Odgen (19)	$C_1=1.58\times10^5$	$C_1=4.12\times10^5$	$C_1=5.06\times10^5$	411.8 ± 39.37
	$C_2=-2.96\times10^5$	$C_2=-7.70\times10^5$	$C_2=-8.23\times10^5$	
	$C_3=1.54\times10^5$	$C_3=4.03\times10^5$	$C_3=3.78\times10^5$	

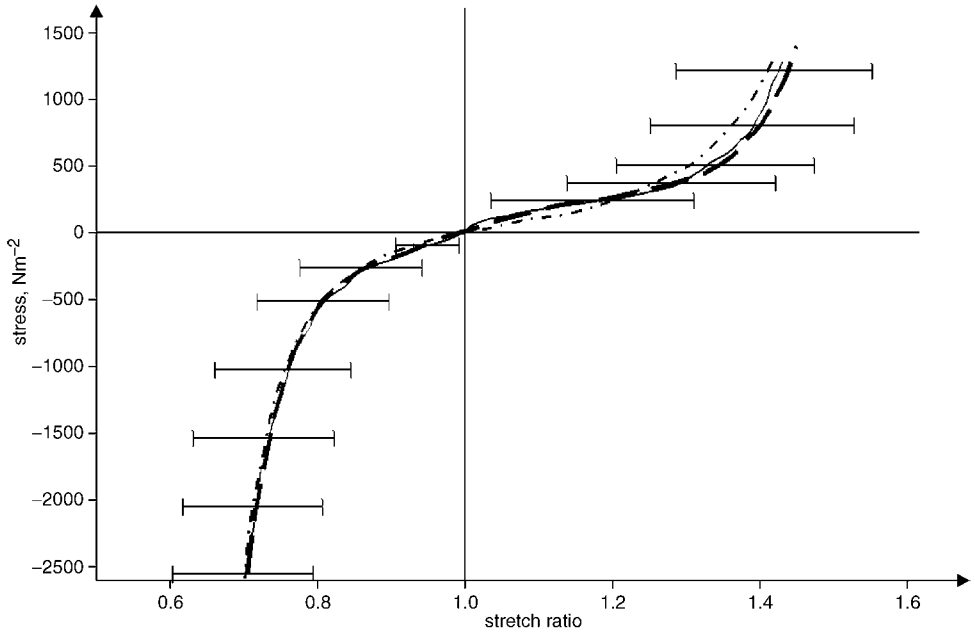

Fig. 8 *Comparison of theoretical and experimental stress (T) stretch (λ) graphs for combined compression and elongation experiments. (—) Mean values of experiments. Standard deviations from mean values are indicated with horizontal bars. (– – –) Theoretical estimation from Mooney–Rivlin (nine-constant) model. (—·—) Theoretical estimation from combined logarithmic and polynomial model*

some of these equations. Exponential and logarithmic models did fit these data, but with relatively high errors. There was no clear advantage in using exponential or logarithmic forms of equations over high-order polynomial equations. The combined energy model and Mooney–Rivlin (nine-constant) model were the only models that could adequately represent these data. Fig. 8 compares the theoretical estimations from the best-fit Mooney–Rivlin (nine-constant) model and the combined polynomial and logarithmic model with the mean value of the experimental stress–strain data.

Generally, the exponential and logarithmic models represented the stress–strain curves better than the polynomial models during compression or elongation. The polynomial models with adequate orders were preferred for combined compression and elongation over exponential or logarithmic models. However, the best constitutive models appeared to be the ones that combined both logarithmic and polynomial forms. These combined logarithmic and polynomial equations provided a good fit for the stress–strain relationships in the tests involving compression followed by elongation, as well as consistently matching the independent compression and elongation data. This combined model was the next best after the Mooney–Rivlin (nine-constant) model in terms of RMSE. As our objective was to obtain relatively simple constitutive equations for fast computer simulation, the smaller number of material constants required in the combined equation was advantageous. Another disadvantage of the Mooney–Rivlin (nine-constant) model was that its material parameters varied widely: a parameter could be positive in one representation and negative in another. This pitfall was typical of polynomial-based constitutive equations. It could cause very different mechanical behaviour in 3D cases. It would also pose serious accuracy issues during numerical analysis, such as the finite element method (HISADA and NOGUCHI, 1995).

Mean values across samples have been used particularly for analysis involving a large number of samples (MILLER and CHINZEI, 1997; MILLER, 2000). In our study, the results from curve-fitting the average stress–strain curve are consistent with those of individual samples. We defined the median stress–strain curve of a porcine liver as the experimental stress–strain curve that was closest to the median value of all the stress–strain curves obtained with samples from that liver. We curve fitted the median stress–strain curve of six porcine livers with the combined logarithmic and polynomial equation and the Mooney–Rivlin (nine-constants) equation. Table 2 shows the parameters and RMSEs for fitting each individual porcine liver. The RMSEs of each curve fit fall within the range defined earlier for both equations. For the Mooney–Rivlin (nine-constant) model, its material parameters varied widely: a parameter could be positive in one representation and negative in another, which happened in all six porcine liver samples. Hence, in view of the smaller number and more consistent material parameters, the combined logarithmic and polynomial model is indeed the better constitutive model.

To validate further the suitability of the combined logarithmic and polynomial equation, we performed separate experiments with small liver samples. The small liver samples had diameters of only 3 mm. Four test samples from one pig, under the same experimental conditions, were tested. Fig. 9 shows the theoretical results and the average for the experimental results for these tests. The theoretical results obtained using this model agreed with the elongation results using these small liver samples.

We repeated the analyses for liver with porcine kidney and brain tissues. The experimental conditions and procedures were the same for all three types of soft tissue. A close fit was possible with the combined logarithmic and polynomial model. The combined logarithmic and polynomial model could model these tissues with similar errors and small deviations

Table 2 Parameters and RMSEs of Mooney–Rivlin (nine-constants) (11) and combined logarithmic and polynomial (22) models in representing combined cycle of compression and elongation experimental data of 6 porcine livers

	Mooney–Rivlin (nine-constants) (11)			Combined logarithmic and polynomial (22)	
	material parameters		RMSE, Pa	material parameters	RMSE, Pa
Liver 1	$C_1 = -0.19 \times 10^4$ $C_2 = 0.22 \times 10^4$ $C_3 = 0.29 \times 10^4$ $C_4 = -0.002 \times 10^4$ $C_5 = -0.41 \times 10^4$	$C_6 = 1.58 \times 10^4$ $C_7 = -0.81 \times 10^4$ $C_8 = 1.07 \times 10^4$ $C_9 = -0.61 \times 10^4$	18.66	$C_1 = -1.67 \times 10^4$ $C_2 = 0.571$ $C_3 = -4.50 \times 10^3$	95.35
Liver 2	$C_1 = -0.11 \times 10^4$ $C_2 = 0.15 \times 10^4$ $C_3 = 0.97 \times 10^4$ $C_4 = -0.49 \times 10^4$ $C_5 = -0.52 \times 10^4$	$C_6 = -3.95 \times 10^4$ $C_7 = -3.41 \times 10^4$ $C_8 = 6.65 \times 10^4$ $C_9 = -4.79 \times 10^4$	24.88	$C_1 = -4.23 \times 10^4$ $C_2 = 0.23$ $C_3 = -4.58 \times 10^3$	90.76
Liver 3	$C_1 = -0.23 \times 10^4$ $C_2 = 0.26 \times 10^4$ $C_3 = 0.63 \times 10^4$ $C_4 = 0.13 \times 10^4$ $C_5 = -0.89 \times 10^4$	$C_6 = 5.54 \times 10^4$ $C_7 = -1.67 \times 10^4$ $C_8 = -2.85 \times 10^3$ $C_9 = 1.36 \times 10^4$	40.15	$C_1 = -6.38 \times 10^2$ $C_2 = 1.62$ $C_3 = -4.14 \times 10^2$	104.69
Liver 4	$C_1 = -0.02 \times 10^4$ $C_2 = 0.053 \times 10^4$ $C_3 = 0.42 \times 10^4$ $C_4 = 0.11 \times 10^4$ $C_5 = -0.46 \times 10^4$	$C_6 = -0.92 \times 10^4$ $C_7 = -0.02 \times 10^4$ $C_8 = 2.54 \times 10^3$ $C_9 = -1.28 \times 10^4$	20.22	$C_1 = -5.94 \times 10^3$ $C_2 = 0.75$ $C_3 = -2.14 \times 10^3$	91.44
Liver 5	$C_1 = 0.11 \times 10^4$ $C_2 = -0.07 \times 10^4$ $C_3 = -0.50 \times 10^4$ $C_4 = 0.25 \times 10^4$ $C_5 = 0.15 \times 10^4$	$C_6 = 3.62 \times 10^4$ $C_7 = -4.38 \times 10^4$ $C_8 = -0.24 \times 10^3$ $C_9 = 1.09 \times 10^4$	45.55	$C_1 = -8.55 \times 10^4$ $C_2 = 0.57$ $C_3 = -9.63 \times 10^3$	105.83
Liver 6	$C_1 = -0.09 \times 10^4$ $C_2 = 0.12 \times 10^4$ $C_3 = 0.19 \times 10^4$ $C_4 = -0.09 \times 10^4$ $C_5 = -0.15 \times 10^4$	$C_6 = -0.25 \times 10^4$ $C_7 = -0.65 \times 10^4$ $C_8 = 2.11 \times 10^3$ $C_9 = -0.95 \times 10^4$	35.37	$C_1 = -1.67 \times 10^4$ $C_2 = 0.28$ $C_3 = -0.19 \times 10^4$	106.67

in material parameters. The polarity of the parameters did not change in the combined model. This demonstrates the suitability of our combined logarithmic and polynomial energy function as the model of choice for soft tissues in general, and liver tissue in particular. Note that experiments with porcine kidney and brain tissues are preliminary at five test samples each.

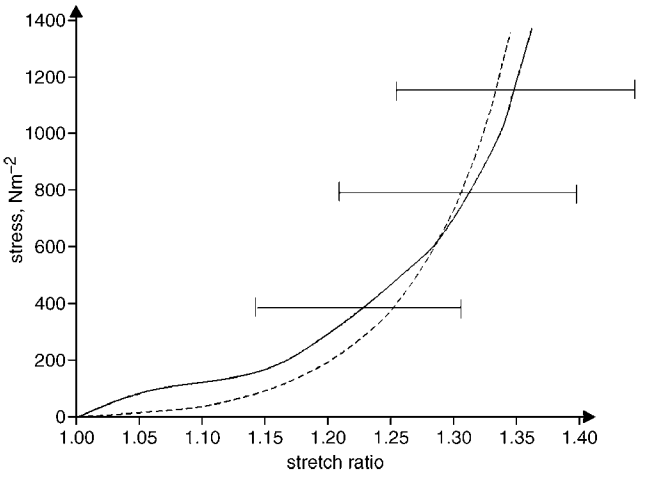

Fig. 9 *Validation of combined logarithmic and polynomial equation using experimental results from smaller samples. Sample diameter was 3 mm, with heights ranging from 5 mm to 6 mm. Number of samples tested was 4. Loading rate was 10 mm min^{-1}. Standard deviations from mean experimental values are indicated with horizontal bars. (—) Experiment; (– – –) Theoretical estimation*

5 Conclusions

In this paper, we have presented our model of the mechanical behaviour of liver based on conventional continuum mechanics, for surgical simulation applications. Our results obtained from *in vitro* uniaxial measurements showed that liver tissue deforms differently under compression and elongation. Thus, instead of relying on separate compression and elongation experiments to define the material properties of liver, we believe that a cycle with both compression and elongation should be used. To the best of our knowledge, this report is the first to express biomechanical properties of biological tissue based on complete cycles of compression and then elongation. The existing constitutive models did not fit this complete cycle of compression and elongation well.

We investigated and confirmed the hypothesis that a constitutive equation with both polynomial and logarithmic forms could best represent the stress–strain relationship of a complete cycle of compression and elongation. In fact, our combined logarithmic and polynomial equation provided an excellent fit over the entire stress–strain curve for separate compression and elongation. Besides demonstrating that our proposed combined logarithmic and polynomial model is the preferred model to represent the liver biomechanical properties, in a preliminary investigation, we found that this theoretical model could represent the stress–strain relationship of other soft tissues, such as porcine brain and kidney tissues.

The value of a model is in predicting actions based on theory of formulated quantitative mechanical properties and principles of physics. It is clear that our experimental and theoretical results agree under the conditions of our experimental design. Unfortunately, biological tissue properties change with disease, and this is the environment in which computer-aided surgery

is performed. We are aiming eventually to introduce parameters of pathology such as stiffness, from diseases such as cirrhosis, and compare cadaver results with experimental predictive data. Under normal conditions, the liver is heavily perfused with blood, both from hepatic arterial and portal venous sources. This perfusion imparts a certain degree of turgidity that is not present in unperfused samples. This will influence the deformation properties. The samples should be infused with solution resembling blood serum at a pressure consistent with that found in the liver. We are enhancing our current experimental measuring system to administrate the infusion process.

We agree with a reviewer that the biphasic model is a possible approach to the integration of the effect of blood pressure that will enhance the realism of surgical simulation of liver therapies. As was also hihlighted by the reviewer, the biphasic model poses a sufficient challenge, both theoretically and experimentally. The resultant biphasic model will possibly be highly complex and interactive, but near real-time computation is impossible with existing hardware. Hence, our work described here is possibly a more practical approach to surgical simulation. A practical application of our work includes simulation of liver deformation from RF needle insertion. In this application, the medical image of a patient's liver was classified into vessels and liver tissues. A finite element model of the liver was then created with elemental material properties defined according to the classified image. The defined material property and modelling of the liver tissues were related to the work described in this paper.

We assumed that liver is an isotropic material in this investigation. In another ongoing study, we have found that the correlation of coefficients obtained from the experimental data with those from theoretical predictions was generally better when transverse isotropy was assumed. This observation is in agreement with a study on constitutive modelling of lung tissue (VAWTER *et al.*, 1980). We have observed that liver tissue has some transverse anisotropy characteristics, and we are currently investigating these characteristics further. We also plan to carry out non-linear finite element simulations based on the tensor forms of our combined logarithmic and polynomial models (ONODERA *et al.*, 2001).

Acknowledgments—This research was supported in part by the Research for the Future Program (JSPS-RTFT99I00904). C. Chui is supported in part by the C&C Foreign Researcher Fund. He is also grateful to Professor J.H. Anderson from The Johns Hopkins University School of Medicine, Baltimore, USA, for many discussions on anatomy, physiology and surgery. The authors also wish to thank the reviewers for their valuable comments.

References

BOGEN, D. (1987): 'Strain-energy description of biological swelling. I Single fluid compartment models', *ASME J. Biomech. Eng.*, **109**, pp. 252–256

BRUYNS, C., and OTTENSMEYER, M. (2002): 'Measuring soft-tissue mechanical properties to support development of a physically based virtual animal model', in DOHI, T., and KIKINIS, R. (Eds): 'Lecture Notes in Computer Science 2488: Medical Image Computing and Computer-Assisted Intervention'. MICCAI 2002, pp. 283–289

CARTER, F. J., FRANK, T. G., DAVIES, P. J., MCLEAN, D., and CUSCHIERI, A. (2001): 'Biomechanical testing of intra-abdominal soft tissue', *Med. Image Anal.*, **5**, pp. 231–236

DAVIES, P. J., CARTER, F. J., and CUSCHIERI, A. (2002): 'Mathematical modelling for keyhole surgery simulation: a biomechanical model for spleen tissue', *IMA J. Appl. Math.*, **67**, pp. 41–67

DAVIES, P. J., CARTER, F. J., ROXBURGH, D. G., and CUSCHIERI, A. (1999): 'Mathematical modelling for keyhole surgery simulations: spleen capsule as an elastic membrane', *J. Theor. Med.*, **1**, pp. 247–262

DEMIRAY, H. (1972): 'A note of the elasticity of soft biological tissues', *J. Biomech.*, **5**, pp. 309–311

FARSHAD, M., BARBEZAT, M., SCHMIDLIN, F., BIDAUT, L., NIEDERER, P., and GRABER, P. (1998): 'Material characterization and mathematical modeling of the pig kidney in relation with biomechanical analysis of renal trauma'. Proc. North American Congress on Biomechanics, Waterloo, Ontario, Canada

FUNG, Y. (1967): 'Elasticity of soft tissues in simple elongation', *American J. Physiology*, **213**, pp. 1532–1544

FUNG, Y. (1993): 'Biomechanics—mechanical properties of living tissues', second edn, (Springer, New York, 1993)

FUNG, Y., LIU, S., and ZHOU, J. (1993): 'Remodeling of the constitutive equation while a blood vessel remodels itself under stress', *ASME J. Biomech. Eng.*, **115**, pp. 453–459

HAWKES, D. J., EWARDS, P. J., BARRATT, D., BLACKALL, J. M., PENNEY, G. P., and TANNER, C. (2003): 'Measuring and modeling soft tissue deformation for image guided interventions', in AYACHE, N. and DELINGETTE, H. (Eds): 'Lecture notes in computer science 2673: surgical simulation and soft tissue modeling', pp. 1–14

HAYASHI, K. (1993): 'Experimental approaches on measuring the mechanical properties and constitutive laws of arterial walls', *ASME J. Biomech. Eng.*, **115**, pp. 481–487

HISADA, T., and NOGUCHI, H. (1995): 'Principle and application of non linear finite element methods (in Japanese)', (Maruzen, Tokyo, Japan, 1995)

KYRIACOU, S. K., SCHWAB, C., and HUMPHREY, J. D. (1996): 'Finite element analysis of nonlinear orthotropic hyperelastic membranes', *Comput. Mech.*, **18**, pp. 269–278

MELVIN, J. W., STALNAKER, R. L., and ROBERTS, V. L. (1973): 'Impact injury mechanisms in abdominal organs', *SAE Trans.*, **730968**, pp. 115–126

MILLER, K. (2000): 'Constitutive modelling of abdominal organs', *J. Biomec.*, **33**, pp. 367–373

MILLER, K., and CHINZEI, K. (1997): 'Constitutive modelling of brain tissue: experiment and theory', *J. Biomech.*, **30**, pp. 1115–1121

MOONEY, M. (1940): 'A theory of large elastic deformation', *J. Appl. Phy.*, **11**, pp. 582–592

MUTHUPILLAI, R., LOMAS, D. J., ROSSMAN, P. J., Greenleaf J. F., MANDUCA, A., and EHMAN, R. L. (1995): 'Magnetic resonance elastography by direct visualization of propagating acoustic strain waves', *Science*, **269**, pp. 1854–1857

ONODERA, K., CHEN, X., and HISADA, T. (2001): 'Identification of biomechanical material properties of soft tissues (in Japanese)'. Proc. Japan Computational Engineering Society Ann. Conf. 2001, Tokyo, Japan

PATHAK, A. P., SILVER-THORN M. B., THIERFELDER, C. A., and PRIETO, T. E. (1998): 'A rate-controlled indentor for *in vivo* analysis of residual limb tissues', *IEEE Trans. Rehabil. Eng.*, **6**, pp. 12–20

SAKUMA, I., NISHIMURA, Y., CHUI, C., KOBAYASHI, E., INADA, H, CHEN, X., and HISADA, T. (2003): '*In vitro* measurement of mechanical properties of liver tissue under compression and elongation using a new test piece holding method with surgical glue', In AYACHE, N., and DELINGETTE, H. (Eds): 'Lecture notes in computer science 2673: surgical simulation and soft tissue modeling', pp. 284–292

SCHMIDLIN, F. R., THOMASON, M., OLLER, D., MEREDITH, W., MOYLAN, J., CLANCY, T., CUNNINGHAM, P., and BAKER, C. (1996): 'Force transmission and stress distribution in a computer simulated model of the kidney: an analysis of the injury mechanisms in renal trauma', *J. Trauma*, **40**, pp. 791–796

TAKAMIZAWA, K., and HAYASHI, K. (1987): 'Strain energy density function and uniform strain hypothesis for arterial mechanics', *J. Biomech.*, **20**, pp. 7–17

TANAKA, T., and FUNG, Y. (1974): 'Elastic and inelastic properties of the canine aorta and their variation along the aortic tree', *J. Biomech.*, **7**, pp. 357–370

VAWTER, D. L., FUNG, Y. C., and WEST, J. B. (1980): 'Constitutive equation of lung tissue elasticity', *ASME J. Biomech. Eng.*, **101**, pp. 38–45

VERONDA, D. R., and WESTMANN, R. A. (1970): 'Mechanical characterizations of ski-finite deformations', *J. Biomech.*, **3**, pp. 111–124

VOSSOUGHI, J. (1995): 'Constitutive modelling of biological materials', in BRONZINO, J. D. (Ed.): 'The biomedical engineering handbook' (CRC Press, 1995), pp. 263–272

XIE, J., ZHOU, J., and FUNG, Y. (1995): 'Bending of blood vessel wall: stress–strain laws of the intima-media and adventitial layers', *ASME J. Biomech. Eng.*, **117**, pp. 136–145
YAMADA, H. (1970): 'Strength of biological materials' (Williams & Wilkins, Baltimore, USA, 1970)
ZOBITZ, M. E., LUO, Z., and AN, K. (2001): 'Determination of the compressive material properties of the supraspinatus tendon', *ASME J. Biomech. Eng.*, **123**, pp. 47–51

Authors' biographies

CHEEKONG CHUI has contributed to over 50 scientific articles in journals and conferences, and is the inventor/co-inventor of 1 US patent and 5 pending patents, mainly in computer-aided surgery. In the Biomedical Precision Engineering Lab at The University of Tokyo, Japan, he focuses on multi-level constitutive modelling of liver tissue for emerging surgical procedures.

ETSUKO KOBAYASHI received her PhD in precision machinery engineering from The University of Tokyo, Japan in 2000. She is currently an assistant professor with the Institute of Environmental Studies, Graduate School of Frontier Sciences, The University of Tokyo. Her research interests are medical robotics and computer-assisted intervention.

XIAN CHEN is an associate professor at The University of Tokyo, Japan. He has been working on computational biomechanics since 1999. His current research interests include multi-physic phenomena of soft tissues, and contact problems in diarthrodial joints using nonlinear finite element method.

TOSHIAKI HISADA received his PhD in mechanical engineering from The University of Tokyo, Japan, in 1979. He is currently a professor, and is heading the Computational Biomechanics Lab at the Institute of Environmental Studies, Graduate School of Frontier Sciences, The University of Tokyo.

ICHIRO SAKUMA received the BS, MS, and PhD degrees in precision machinery engineering from The University of Tokyo, Tokyo, Japan, in 1982, 1984, and 1989, respectively. He was a research associate in The Department of Precision Machinery Engineering at The University of Tokyo from 1985 to 1987. He was a Research Instructor at Baylor College of Medicine, Houston, Texas, USA from 1990–1991. He was an associate Professor at The Department of Applied Electronic Engineering, Tokyo Denki University, Saitama, Japan, from 1992 to 1998. He was an Associate Professor at the Department of Precision Engineering in the Graduate School of Engineering, as well as at the Institute of Environmental Studies at the Graduate School of Frontier Sciences, at The University of Tokyo, from 1998 to 2001. He is currently a professor at the Institute of Environmental Studies at The University of Tokyo. His research interests are in bio-medical instrumentation, simulation of biomedical phenomena, computer-assisted intervention, and surgical robotics.